Palaeomagnetism, rock magnetism and AMS of the Cabo Magmatic Province, NE Brazil, and the opening of South Atlantic

Article *in* Geophysical Journal International · November 2009

DOI: 10.1111/j.1365-246X.2009.04333.x

5 authors, including:

Eric Font
University of Lisbon
108 PUBLICATIONS **1,565** CITATIONS
SEE PROFILE

Marcia Ernesto
University of São Paulo
100 PUBLICATIONS **3,704** CITATIONS
SEE PROFILE

Pedro Silva
Instituto Politécnico de Lisboa
60 PUBLICATIONS **969** CITATIONS
SEE PROFILE

Paulo de Barros Correia
Federal University of Pernambuco
15 PUBLICATIONS **149** CITATIONS
SEE PROFILE

Geophys. J. Int. (2009) **179,** 905–922 doi: 10.1111/j.1365-246X.2009.04333.x

Palaeomagnetism, rock magnetism and AMS of the Cabo Magmatic Province, NE Brazil, and the opening of South Atlantic

E. Font,[1] M. Ernesto,[1] P. F. Silva,[2,3] P. B. Correia[4] and M. A. L. Nascimento[5]

[1]*Department of Geophysics, University of São Paulo, Brazil. E-mail: font_eric@hotmail.com*
[2]*IDL-FCGUL, Faculdade de Ciências de Lisboa, Portugal*
[3]*ISEL/DEC, Lisboa, Portugal*
[4]*Universidade Federal de Pernambuco, Recife, Brazil*
[5]*CPRM–Geologic Survey of Brazil, Natal, Brazil*

Accepted 2009 July 10. Received 2009 July 10; in original form 2008 September 26

SUMMARY

Reconstruction of the South Atlantic opening has long been a matter of debate and several models have been proposed. One problem in tracing properly the Atlantic history arises from the existence of a long interval without geomagnetic reversals, the Cretaceous Normal Superchron, for which ages are difficult to assign. Palaeomagnetism may help in addressing this issue if high-quality palaeomagnetic poles are available for the two drifting continental blocks, and if precise absolute ages are available. In this work we have investigated the Cabo Magmatic Province, northeastern Brazil, recently dated at 102 ± 1 Ma (zircon fission tracks, Ar^{39}/Ar^{40}). All volcanic and plutonic rocks showed stable thermal and AF demagnetization patterns, and exhibit primary magnetic signatures. AMS data also support a primary origin for the magnetic fabric and is interpreted to be contemporaneous of the rock formation. The obtained pole is located at 335.9°E/87.9°S ($N = 24$; $A_{95} = 2.5$; $K = 138$) and satisfies modern quality criteria, resulting in a reference pole for South America at ∼100 Ma. This new pole also gives an insight to test and discuss the kinematic models currently proposed for the South Atlantic opening during mid-Cretaceous.

Key words: Magnetic fabrics and anisotropy; Palaeomagnetism applied to tectonics; Rock and mineral magnetism; Atlantic Ocean; South America.

1 INTRODUCTION

Reconstruction of the South Atlantic opening has long been a matter of debate, and recently gained a renewed attention due to economic interests. Several models for the Atlantic evolution have been proposed, most of them based on the recognition of sea floor magnetic anomalies and fracture zones (Eagles 2007, and references therein). More recently, new information has been added in order to better define Euler poles and the amount of rotation for each considered age (Shaw & Cande 1990; Eagles 2007). Models considering intraplate deformations was proposed initially by Unternehr *et al.* (1988) and then improved by other authors (Eagles 2007) in order to overcome the misfit between South America and Africa in a pre-drift configuration.

One problem in tracing properly the Atlantic history arises from the existence of a long (∼40 Myr) interval without geomagnetic reversals, the Cretaceous Normal Superchron (CNS). Recently, He *et al.* (2008) on the basis of $^{40}Ar/^{39}Ar$ dating and palaeomagnetic data demonstrated that the M0r anomaly is actually approximately 121 Ma in age, placing the lower limit of the CNS slightly younger than previously reported (∼124 Ma; Gradstein *et al.* 2004). Actually short reversed events have already been reported at ages 120–115 Ma (Vandenberg *et al.* 1978; Tarduno 1990; Gvirtzman *et al.* 1996; Poornachandra Rao & Mallikharjurna Rao 1996), ∼105 Ma (Tarduno *et al.* 1992) and ∼95 Ma (Irving & Archibald 1990) for continental rocks and Deep Sea Drilling Project sites. However, the seafloor record does not provide the necessary resolution to detect such short lasting polarity events.

Palaeomagnetism may help in addressing this issue if high-quality palaeomagnetic poles are available for the two drifting continental blocks and if absolute ages are precise. Those conditions can be better achieved for poles derived from igneous rocks. In South America, the best-known possibility is the Cabo Magmatic Province (CMP), northeastern Brazil of mid-Cretaceous age. Data from this province had already been published by Schult & Guerreiro (1980), known as the Cabo de Santo Agostinho pole. However, their results may be questioned for the limited number of investigated sites, absence of thorough magnetic mineralogy investigation, and no principal component analysis (Kirschvink 1980) to identify and isolate primary magnetization components. This method is nowadays a fundamental criterion to assess the reliability of palaeomagnetic poles.

In this work, we present a detailed palaeomagnetic work of the CMP. We investigated all igneous rocks including the Cabo granite

and monzonite, which were not studied in the previous work. Detailed rock magnetism was performed as the near equator location of the province favours deep weathering. Data on anisotropy of magnetic susceptibility is also discussed aiming mainly to investigate eventual internal deformation in the intrusive rocks, and to detect non-observable tilting.

2 GEOLOGICAL SETTING

The CMP situated near the city of Recife, northeastern Brazil, is constituted by several types of volcanic, plutonic and sedimentary rocks with ages ranging from Mesozoic to Cenozoic. Its genesis is related to the tectono-sedimentary evolution of the Pernambuco Basin which took place during the break up of Western Gondwana and the opening of South Atlantic. The Pernambuco Basin is limited by the Pernambuco lineament on the north, the Maragogi High on the south and the basement rocks (gneissic-migmatic complexes) on the west (Fig. 1). The eastern onshore portion is composed of a lowermost Aptian to Albian rift phase.

The stratigraphy of the Pernambuco Basin is represented by the Cabo Formation, made of Aptian-Albian conglomerates (coarse sandstones with silts and shales) related to the rift phase covered by

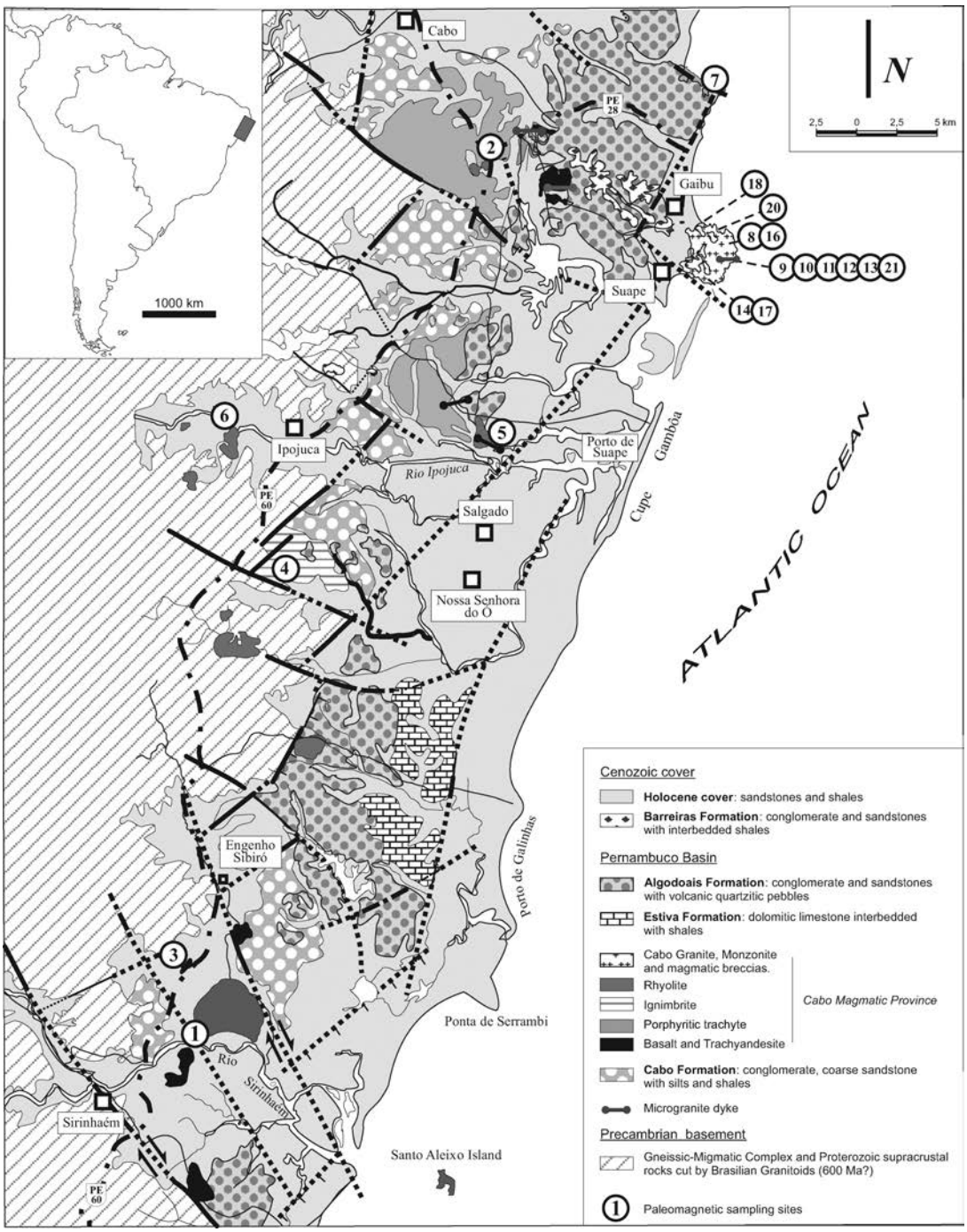

Figure 1. Geological map (modified from Lima Filho 1998; Nascimento 2003) of the Pernambuco Basin and its location in South America (left-hand inset). Numbers indicate palaeomagnetic sites.

Table 1. Characteristic magnetic components of CMP rocks and corresponding VGPs; D (°), Declination; I (°), Inclination; N, number of samples for the means; α_{95} (A_{95}) and k (K) are Fisher's (1953) statistical parameters for the mean directions (VGPs).

		Characteristic magnetization						Virtual geomagnetic poles			
Sites	Lithology	Comp.	N	D (°)	I (°)	α_{95}	k	Long (°E)	Lat (°)	A_{95}	K
EC1-1	Rhyolite	A	8	13.7	−22.8	6.2	80	249.8	−76	5.1	103
EC1-2	Rhyolite	A	6	344.3	−22.9	6.6	105	41.3	−74.2	5.4	136
EC1-3	Rhyolite	A	7	4.0	−24.2	5.0	144	281.5	−84.3	6	110
EC2	Rhyolite	B	4	286.4	−18.4	3.7	610	47.6	−17.4	2.9	793
EC3	Trachy-andesite	A	5	359.1	−10.2	8.0	92	130.3	−86.5	9.1	70
EC4	Ignimbrites	A	7	8.7	−21.8	6.1	100	256.8	−80.8	7.2	76
EC5	Rhyolite	A	11	1.9	−14.2	4.0	133	212.5	−88	3.1	173
EC6-1	Rhyolite	B	8	293.4	−24.8	7.0	63	44.4	−24.6	5.8	82
EC6-2[a]	Rhyolite	C	6	294.8	50.5	4.8	199	271	16.4	5.4	153
EC6-3	Rhyolite	A	4	0.5	−8.5	7.5	150	151.8	−85.9	8.5	115
EC6-4[a]	Rhyolite	A	2	330.9	−17.9	18.9	177	50.5	−61.2	14.9	230
EC6-5[a]	Rhyolite	C	7	335.6	51.5	8.1	56	296.1	43.6	13.3	43
EC6-6	Rhyolite	A	15	352.2	−20.1	3.9	98	39.9	−82.1	4.6	75
EC7-1[a]	Trachyte	A	9	338.8	−19.6	3.5	215	48.5	−69	4.2	165
EC7-2	Trachyte	B	4	289.7	−19.5	9.1	104	47.4	−20.7	7.3	135
EC7-3	Trachyte	A	7	1.1	−20.3	4.6	172	298.7	−87.6	3.7	224
EC7-4	Trachyte	A	9	350.9	−14.8	4.0	165	59.3	−80.9	3.1	215
EC7-5	Trachyte	A	7	0.6	−15.3	5.0	149	194.4	−89.2	3.9	194
EC7-6	Trachyte	A	14	1.2	−17.4	3.5	130	262.2	−88.7	4.1	100
EC8	Granite	A	6	3.3	−24.2	5.0	178	290.5	−84.3	6	137
EC9	Microgranite	A	3	355.1	−15.0	14.1	77	59	−85.1	16.3	59
EC10-1	Monzonite	A	4	357.0	−29.8	5.6	275	345.8	−81.8	4.8	357
EC10-2	Monzonite	B	6	306.0	−27.0	9.3	52	43.4	−36.8	7.8	68
EC11	Microgranite	A	6	8.1	−29.0	5.5	150	279.1	−79.1	6.9	115
EC12	Monzonite	A	11	1.9	−31.6	4.7	96	313.3	−81.1	6.1	74
EC13	Granite	A	14	4.9	−23.7	4.7	72	275.4	−83.7	3.9	94
EC14	Granite	A	13	356.3	−18.9	5.5	58	34.3	−86.1	4.4	75
EC16	Granite	A	4	354.5	−23.8	9.6	92	17.5	−83.2	10.5	70
EC17	Granite	A	5	1.4	−20.8	5.3	210	295.3	−87.2	5.7	161
EC18	Granite	A	17	356.6	−20.1	4.9	54	19.5	−85.9	4.7	70
EC20	Granite	A	7	353.9	−17.4	6.7	83	49.4	−83.9	6.5	108
EC21	Granite	A	4	0.3	−21.1	11.5	64	318.5	−87.4	9.3	84
Comp. A	Mean		24	359.6	−20.4	3	99	335.9	−87.9	2.5	138
Comp. B	Mean		4	293.7	−22.6	10.1	84	45.9	−24.8	9.9	87

[a]Excluded from the mean.

200 m of the siliciclastic alluvial fans (conglomerate, silt and shale) and lacustrine sediments of the Estiva and Algodoais formations (Lima Filho 1998).

The Pernambuco basin was affected by an intense magmatism (Nascimento 2003) represented by sills and lava flows cutting the clastic sediments of the Cabo Formation. They correspond to trachy-andesites, andesites, rhyolites, ignimbrites and porphyric trachyte and fine granites which have been grouped by Nascimento (2003) into a transitional to alkaline suite (basalts to trachy-andesites, trachytes and monzonites) and an alkaline, strongly fractionated, acidic volcano-plutonic association, (ignimbrite flows, fine- to medium-grained rhyolites, a high-level granite and later rhyolites). Geochemical composition of these rocks suggests an evolution trough low-pressure fractional crystallization of crustal melts for trachytes and other acidic rocks, whereas basalts, trachy-andesites and monzonites evolved by partial melting from a mantle source. According to Nascimento (2003) the tectonic evolution of the Pernambuco Basin comprised an astenospheric rising with subsequent crustal rifting with extension predominantly oriented NW–SE. The lowermost sequences of the Cabo Formation were deposited during the final stage of the rifting marked by the intrusion of the acid and basic magmas of the CMP. Structural features of CMP rocks are mostly originated by brittle deformation and barely represented by minor faults and fractures, which caused no significant tilting of the magmatic bodies.

The Cabo de Santo Agostinho Granite represents the major sampling area of the CMP, essentially located on the coast between Gaibú and Suape beachs. It consists of alkaline-feldspar leucocrate fine granites, which include two varieties (granite and microgranite) both with similar mineralogy. Rare Earth Elements data indicate enrichment of heavy elements and depletion in light elements suggesting origin from a granitic magma rich in alkaline and H_2O, and formed from partial fusion of the lower continental crust or mantle (Nascimento 2003). The Cabo de Santo Agostinho granites are neither deformed nor metamorphosed.

Magmatic rocks of the CMP have been dated by Rb-Sr (Long *et al.* 1986), K-Ar (Vandoros *et al.* 1966) and Ar^{39}/Ar^{40} (Lima Filho & Szatmari 2002) methods giving ages ranging from 111 to 85 Ma (Albian to Santonian). More recently Nascimento (2003) reported Ar^{39}/Ar^{40} ages and fission in zircon ranging from 104.4 ± 0.8 to 100.3 ± 0.6 Ma, and clustering around 102 ± 1 Ma. The various lithotypes in the province exhibit no significant age differences. However, for the granite, Lima Filho & Szatmari (2002) reported an Ar^{39}/Ar^{40} whole rock age of 111.2 ± 1.3 Ma. This age is significantly older than the single crystal (three feldspars, three biotites and three amphiboles) laser incremental heating method

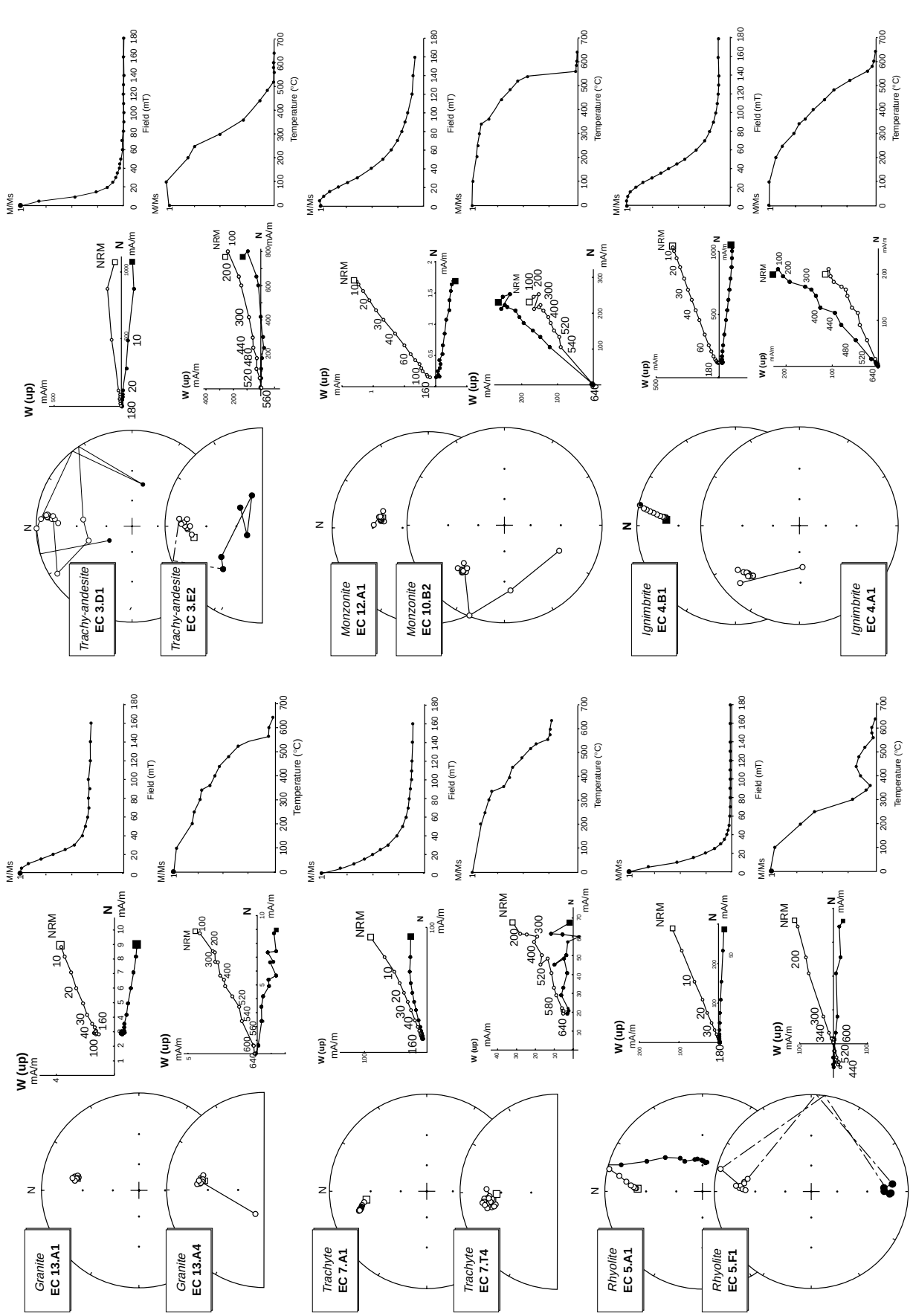

Figure 2. Typical AF and thermal demagnetization plots of CMP rocks. (on the left-hand side) Stereographic projections with closed (opened) symbols indicating reverse (normal) component. (centre) Orthogonal plots with solid (open) data points indicating vector end points projected onto the horizontal (vertical) plane. (on the right-hand side) Demagnetization intensity plots.

used to obtain the ∼102 Ma leading Nascimento (2003) to propose a crustal contamination in the whole rock result. The ∼102 Ma age is interpreted as corresponding to the cooling stage and to the maximal rifting phase of the Pernambuco basin.

3 SAMPLING AND METHODS

Cylindrical samples were collected with the aid of a manual gasoline-powered rock drill. Sample orientation was performed by both magnetic and sun compasses. From each palaeomagnetic site (outcrop) at least three cylinders were taken which were then cut into standards specimens of 2.2 cm diameter and 2.2 cm height. A total of 21 localities corresponding to 32 independent palaeomagnetic sites or cooling units (more than 260 samples) were sampled including trachytes, trachyte-andesites, rhyolites and one ignimbrite (Fig. 1, Table 1). Sites of the Cabo granite and monzonite were distributed around the exposed area near the sea.

In order to reduce viscous overprints on the characteristic magnetization, samples were stored in a low-field chamber for three months. Palaeomagnetic directions were isolated after alternating field (AF) and thermal demagnetization treatments using several progressive steps. AF demagnetization and remanence measurements were performed in a 2G-cryogenic magnetometer coupled to a tri-axial AF-demagnetizer. Some additional measurements were performed in a JR6 magnetometer. Both equipments were housed in a magnetically shielded room at University of São Paulo (ambient field <1000 nT). Thermal demagnetization was performed in a magnetic measurements furnace (peak temperature within ±5 °C). Principal component analysis (Kirschvink 1980) was used to determine magnetic components, and mean directions were evaluated by means of Fisher's (1953) statistics.

Frequency-dependence of magnetic susceptibility was obtained in a Bartington MS2 dual-frequency (470 and 4700 Hz) alternating-current bridge on whole rock specimens. IRMs were induced in a Pulse Magnetizer (MMPM 10) while for the Lowrie–Fuller and Cisowski tests samples were first demagnetized at 200 mT and then subjected to an AF peak field of 160 mT plus a DC field of 0.1 mT (ARM acquisition). After AF demagnetization, samples acquired an IRM up to 160 mT and were subsequently stepwise demagnetized at fields up to 160 mT. Thermomagnetic curves were obtained with a KLY4 Kappabridge apparatus in an Argon-controlled atmosphere. scanning electron microscopy (SEM) observations and Energy Dispersive Spectra (EDS) analysis were performed on carbon-coated rock fragments with a Jeol JSM-6360LV microscope coupled to a Noran Instrument EDS analyser. Anisotropy of Magnetic Susceptibility (AMS) was measured in a KLY3 Kappabridge, although some of rocks were also measured in a Minisep.

4 PALAEOMAGNETIC RESULTS

Samples from the CMP showed large variations ($5 - > 10^4$mA m^{-1}) of natural remanent magnetization. Granites showed the lowest NRM values ($\sim 10^1$mA m^{-1}) while monzonites exhibited the largest variation and highest values (2.13–10^4 mA m^{-1}); intermediate values ($\sim 10^2$ mA m^{-1}) were found for rhyolites and trachytes whereas trachy-andesites presented values one order of magnitude higher ($\sim 10^3$ mA m^{-1}). During AF and thermal demagnetization procedures the majority of samples showed stable demagnetization patterns (Fig. 2), although AF cleaning was more efficient in revealing characteristic components.

Granites (sites EC8–13-14–16-17–18-20–21), microgranites (sites EC9–11) and Trachytes (site EC7) showed similar magnetic behaviour characterized by a single, stable N–S component with inclinations of 20°–25° (Fig. 3). AF demagnetization intensity plots are characteristic of low to medium coercive magnetic minerals (Fig. 2). At 160 mT more than 30 per cent of the total remanence persists indicating the presence of a higher coercive phase (hematite). The mixture of magnetite and hematite is confirmed by the thermal demagnetization intensity plot for which unblocking temperatures are close to 560 °C (titanomagnetite) and 640 °C. A slight hump at 350 °C suggests a low contribution of maghemite.

Rhyolites (sites EC1–2-5–6) showed stable uni- and multivectorial demagnetization patterns; a low coercivity magnetic component was isolated between 0 and 10 mT corresponding to a viscous remanent magnetization (VRM) significantly different from the present-day field. For most of the samples more than

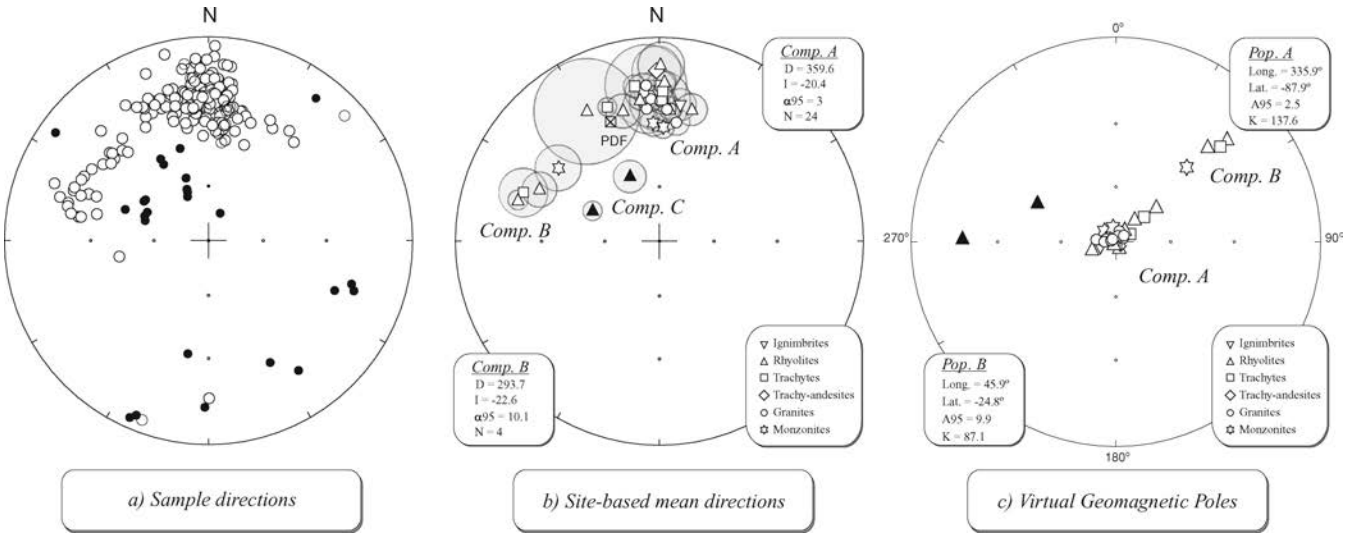

Figure 3. Stereographic projections of: (a) sample-based mean directions, (b) site-based mean directions for each rock type, (c) VGPs on a polar projection. Boxes show declination (D) and Inclination (I) values and statistical parameters (α_{95} and N = number of samples used for mean). Samples excluded for mean calculation are included. The position of the local present-day field is also indicated. [Correction made after online publication 24 September 2009: panel (c) has been replaced.]

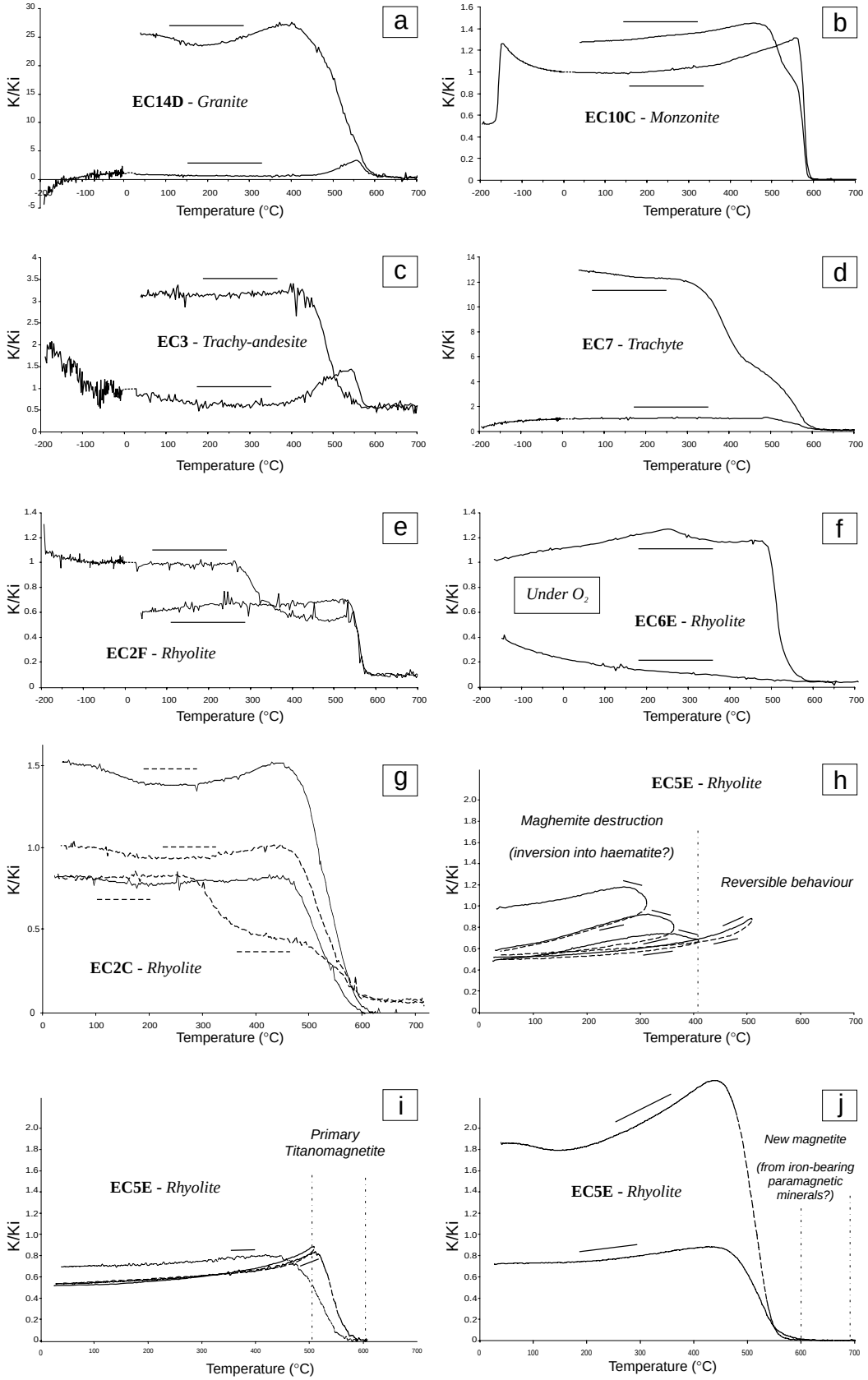

Figure 4. Thermomagnetic analyses of CMP rocks. Heating and cooling are indicated by arrows. (a–e) LT and HT thermomagnetic analyses of whole CMP rocks under Ar-controlled atmosphere; HT thermomagnetic curves of rhyolite samples (f) under ambient (O_2) atmosphere and (g) after two successive heating step until 700 °C under Ar-atmosphere. Dashed lines correspond to the first heating phase and solid lines to the second one. (h) Stepwise thermomagnetic analyses in Ar-atmosphere at 250, 300, 350, 400 and 500 °C, (i) 600 °C and (j) 700 °C.

95 per cent of the remanence was removed after 160 mT or temperatures of 580 °C suggesting that titanomagnetite is the main magnetic carrier. Maghemite is also ubiquitous as noted by the slight inflections at around 350 °C (Fig. 2). Unblocking temperatures above 640 °C suggest presence of hematite but as this mineral was not depicted in AF cleaning we interpreted it to be the product of maghemite inversion during heating. In some cases this inversion was followed by a change in remanence direction resulting in an antipodal component (Fig. 2; sample EC5.F1) erased above 500 °C. In the companion sample EC5.A1 (Fig. 2) the same positive inclination component was noticed during AF demagnetization when no mineralogical transformation occurs.

Trachy-andesite (site EC3) showed very stable magnetic component up to high fields and temperatures (Fig. 2). A VRM was removed after cleaning up to 100 °C and the characteristic remnant magnetizations clustered at N0° with a negative inclination of about 15° (Fig. 3). Unblocking temperatures of 520 °C, as well as the shape of the AF demagnetization curves, suggest Ti-bearing magnetite as the main magnetic carrier.

Monzonites (sites EC10 and EC12) and ignimbrites (site EC4) showed a very stable uni-vectorial component with characteristic directions mainly plotting to approximately N00°/−30° (Fig. 3). The remanence is carried by titanomagnetite with a low contribution of maghemite in some monzonites (sample EC10, Fig. 2). Hematite is also depicted but not as abundant as in granites and trachytes.

All identified magnetization directions are seen in Fig. 3; most of them cluster near a $N \pm 30°$ with negative inclinations (component A) which correspond to a normal polarity field displaced from the local present field. Four sites of different lithologies showed oblique directions with negative inclinations (component B). Various samples allowed calculation of a positive inclination remanence (component C), which however, may be related to weathering or self-reversal as discussed in Section 6. In most cases they are scattered, and do not characterize a ChRM, excepting for sites EC6-2 and EC6-5 which corresponds to different levels of a thick rhyolite outcrop in which remanence varies from component A to B, from bottom to top, respectively. Although component C may be not of primary origin, the magnetic behaviour defined by the other two components is consistent with a transitional geomagnetic field. The CMP formed in a relatively short time interval (∼4 Ma), and is completely inserted within the Cretaceous Normal Superchron (124.5–84 Ma, Gradstein *et al.* 2004). However, short reversed events in this superchron have already been reported at various times (Vandenberg *et al.* 1978; Irving & Archibald 1990; Tarduno 1990; Gvirtzman *et al.* 1996; Poornachandra Rao & Mallikharjuna Rao 1996) including some events at about 105 Ma (Tarduno *et al.* 1992) which could be related to the CMP possible record.

Virtual Geomagnetic Poles (VGPs) corresponding to each site mean direction are plotted in Fig. 3 as south poles. They group tightly near the geographic pole, but a path along a nearly constant meridian (∼45°) is noticed toward those VGPs corresponding to component B at low latitudes (∼20°). We have used the recursive method of Vandamme (1994) to establish a cut-off dispersion value for the VGP distribution. In this method, the cut-off angle is calculated from the angular standard deviation of the VGP distribution and the final cut-off is obtained by iteration until the angle between the furthest VGP and the mean (Dmax) is less than the cut-off angle. Considering all data (of component A) the final cut-off angle (cut-off $= 17.5° > D_{max} = 15.1$) was obtained for $N = 24$. The resulting palaeomagnetic pole for CMP rocks is then located at 335.9°E/87.9°S ($N = 24$; $A_{95} = 2.5°$; $K = 138$).

5 MAGNETIC MINERALOGY

5.1 Thermomagnetic curves

Thermomagnetic analyses in high (HT) and low (LT) temperatures under Argon-controlled and ambient atmosphere have been done at least for one sample per site (Fig. 4). LT thermomagnetic analyses under Ar-controlled atmosphere had revealed a major contribution of paramagnetic minerals in most samples as indicated by the linear aspect of the LT curve. Sample EC10C (monzonite) show a clear Verwey transition at around −150 °C pointing to presence of multidomain magnetite or eventually equidimensional SD magnetite as suggested by the PSD-SD response in the Lowrie–Fuller test (Fig. 7). HT analyses show major drops in susceptibility at around 580 °C depending on rock type (Fig. 4) indicating magnetite as the main ferromagnetic carrier. However, unblocking temperatures lower than 580 °C (Fig. 2) along with significant Ti peaks in EDS spectra (see later) point to the presence of titanomagnetite rather than nearly pure magnetite. Presence of titanomagnetite in granites and trachy-andesites is confirmed by a prominent Hopkinson peak at around 560 °C characteristic of SD magnetite (Figs 4a and c). In addition, hematite/titanohematite is present in granites and trachytes and identified by the persistence of a small percentage of magnetic susceptibility after 580 °C. In rhyolites, omnipresence of titanomaghemite is revealed by an abrupt decrease of magnetic susceptibility between 300 and 350 °C (Figs 4e–j).

Except for monzonite (EC10), which shows quasi reversible behaviour, all rocks suffer considerable mineralogical transformations during heating processes. Under ambient atmosphere, rhyolites show an irreversible behaviour with a magnetic susceptibility that is considerably reduced after cooling below 700 °C suggesting that under high O_2 fugacity, maghemite and magnetite were totally oxidized at 700 °C into hematite (Fig. 4f). Under Ar-atmosphere, two successive stages of heating lead to the destruction of all titanomaghemite (Fig. 4g). Using stepwise heating, this titanomaghemite disappears below 400 °C and curves then became reversible (Fig. 4h). Above 400 °C susceptibility slightly increases, probably due to the Hopinkson effect, and fall at 560–580 °C (Fig. 4i). After cooling below 700 °C, susceptibility increases considerably suggesting formation of new magnetite probably due to transformation of iron-bearing paramagnetic minerals (Fig. 4j). These results indicate that CMP rocks still preserve their primary TRM as no major thermal event affected the area. However, to the primary TRM a chemical remanent magnetization (CRM) acquired by exsolved hematite was added in granite while, in other rocks, a CRM acquired during low-temperature oxidation is also carried by maghemite and Ti-maghemite.

5.2 IRM analyses

5.2.1 IRM acquisition curves

Isothermal remnant magnetization acquisition curves were obtained for more than 15 samples at fields up to 2 T (Fig. 5). Data were treated by the cumulative log-Gaussian method (Robertson & France 1994) using the software of Kruiver *et al.* (2001) (Fig. 5; Table 2). Most CMP rocks are characterized by a bimodal distribution of magnetic phases, probably magnetite and hematite except for trachy-andesite, ignimbrite and some rhyolite and monzonite samples for which only a low coercive phase is present (Fig. 6a). The lower coercive phase presents a narrow range of DP values interpreted to correspond to a homogenous population of magnetite

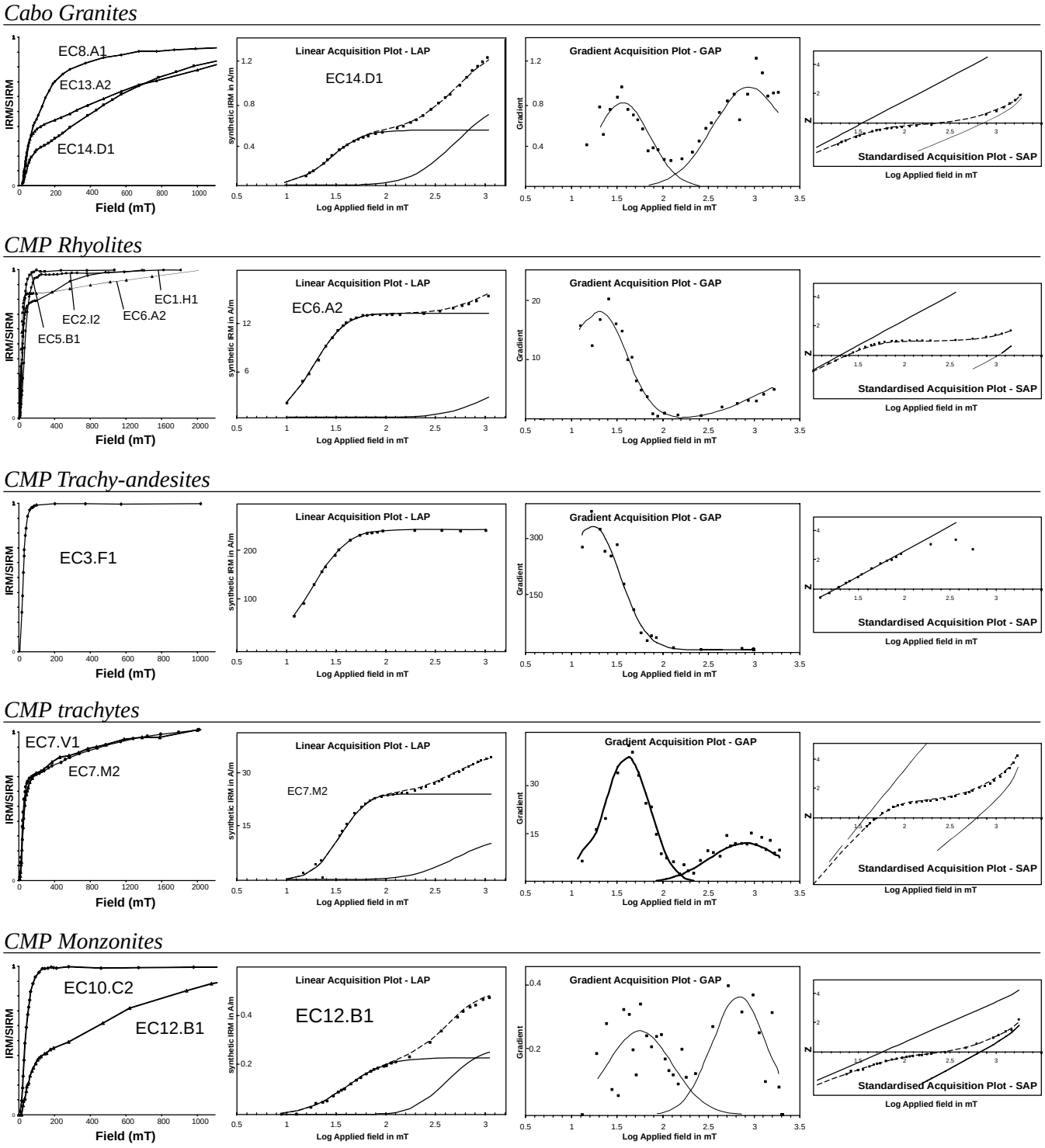

Figure 5. IRM acquisition curves for CMP rocks and treatment by cumulative log-Gaussian (Robertson & France 1994) functions using the software developed by Kruiver *et al.* (2001).

(Fig. 6b). Distinctly, the higher coercive phase (>100 mT), probably corresponding to hematite, presents a wide range of DP values (0.20–0.40) indicating different grain sizes.

5.2.2 Lowrie–Fuller and Cisowski tests

Most samples of the Cabo granites gave SD-like response in the Lowrie–Fuller test with typical convex shape of IRM and ARM demagnetization curves (Fig. 7). Granite rocks show MD behaviour with unsaturated state at IRM acquisition and demagnetization (Fig. 7, EC8.A2). For other rocks the low coercive phase is saturated and hematite contribution is minor. Most IRM and ARM demagnetization curves are similar even with distinct concave and convex shapes suggesting that mixtures of PSD and SD particles dominate the magnetic mineralogy. All samples submitted to the Cisowski (1981) test exhibit R (interaction degree) values less than

Table 2. Values of SIRM (A m^{-1}), $B_{1/2}$ (mT) and Dispersion parameter (DP) after cumulative log-Gaussian (Robertson & France 1994) treatment using the software developed by Kruiver *et al.* (2001).

Samples	Comp.	Contribution (per cent)	SIRM (A m^{-1})	*B*1/2 (mT)	DP
This study					
EC3.F1	1	100.00	242.00	17.78	0.29
EC4.I1	1	100.00	110.00	50.12	0.28
EC2.I2	1	100.00	41.50	63.10	0.29
EC5.B1	1	100.00	210.00	39.81	0.25
EC10.C2	1	100.00	96.00	35.48	0.28
EC1.H1	1	80.69	18.80	31.62	0.28
	2	19.31	4.50	446.68	0.25
EC6.A2	1	72.53	13.20	19.95	0.29
	2	27.47	5.00	1995.26	0.40
EC7.M2	1	66.67	24.00	38.90	0.25
	2	33.33	12.00	794.33	0.40
EC7.V1	1	68.18	30.00	44.67	0.27
	2	31.82	14.00	794.33	0.30
EC8.A1	1	59.38	0.95	44.67	0.30
	2	40.63	0.65	199.53	0.22
EC12.B1	1	46.00	0.23	56.23	0.36
	2	54.00	0.27	707.95	0.30
EC13.A2	1	25.00	0.65	39.81	0.28
	2	75.00	1.95	630.96	0.35
EC14.D1	1	38.71	0.60	35.48	0.30
	2	61.29	0.95	891.25	0.40

$\sim$0.3 indicating high interactions between SD particles with Hcr $<$ 40 mT, typical of low coercive magnetic phases.

5.2.3 NRM:IRMs

The comparison of the magnitude and demagnetization patterns of the NRM with those of saturation IRM provide a good proxy for distinguishing primary and secondary magnetizations (Fuller *et al.* 1988; Fuller *et al.* 2002): NRM/IRM ratios of the order of 10^{-2} are indicative of thermal remanent magnetization; smaller values implying secondary magnetization (Fuller *et al.* 2002). All plutonic and volcanic rocks of the CMP showed roughly straight lines near the limit of 10^{-2} (Fig. 8) indicating remanence of thermal origin. Curves showing a slight flattening for high demagnetization fields (60–100 mT) may correspond to a mixture with a higher coercive phase like hematite. As in the case of the Lowrie–Fuller test, only low coercive phases could be analysed and hematite contribution could not be discussed.

Table 3. Frequency-dependence of susceptibility of the CMP rocks.

Rock-type	Samples	Kfd
Rhyolite	EC1.D2	1.31
	EC2.D2	1.82
	EC5.G3	0.36
	EC6.I2	0.00
Basalt	EC3.D2	−2.08
Ignimbrite	EC4.H2	−2.37
Trachyte	EC7.S3	0.78
Granite	EC8.A2	25.00
	EC13.B1	75.00
	EC14.C3	40.00
Monzonite	EC10.D1	4.88
	EC12.C2	7.41

5.3 Frequency-dependence of susceptibility (Kfd)

Frequency-dependent susceptibility measurements infer the presence of ultrafine particles near the superparamagnetic (SP) domain. In our samples, Kfd values vary from −2.4 to more than 70 depending of rock-type (Table 3). For rhyolites, trachy-andesites and trachytes, superparamagnetic particles are rare or absent. Monzonite show intermediate values indicating low to medium contribution of SP particles. Granites present the higher Kfd values (25–70 per cent)

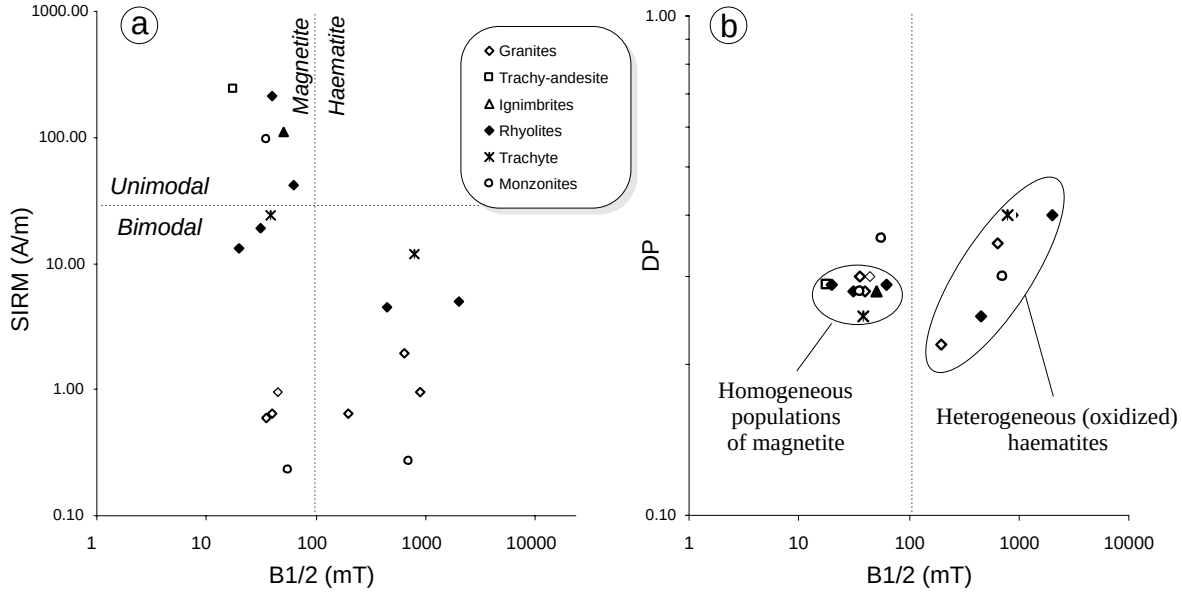

Figure 6. (a) SIRM versus B1/2 plot illustrating uni- and bi-modal distributions of magnetic phases in CMP rocks: except for trachy-andesite, ignimbrite and some monzonite and rhyolite samples, most rocks present a bimodal distribution of magnetic phases interpreted to correspond to magnetite and hematite. (b) DP versus B1/2 plot distinguishing the relative homogeneity of magnetite populations (low dispersion of DP values) compared to hematite. The field limit between magnetite/hematite is arbitrarily stated at around 100 mT.

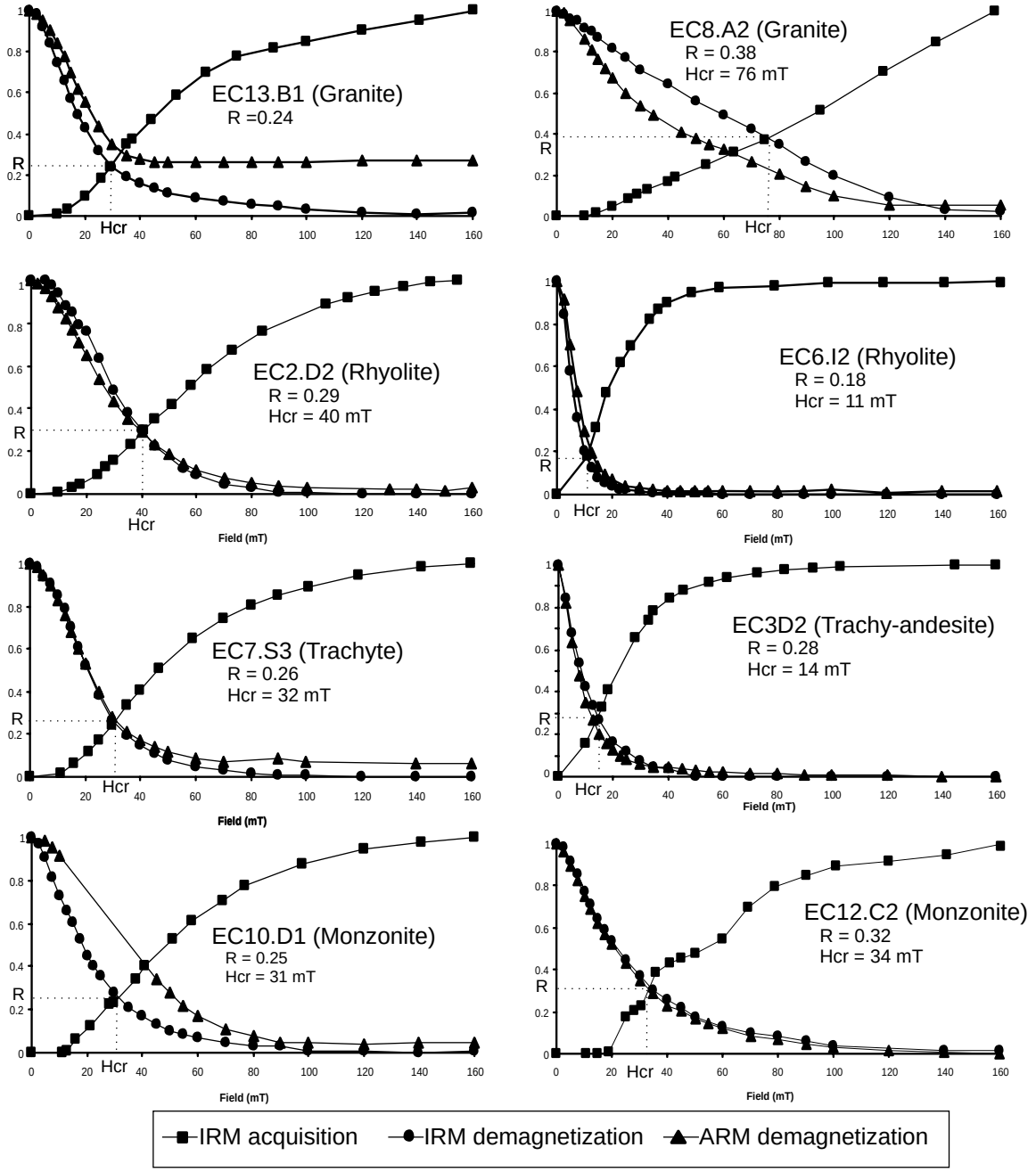

Figure 7. Lowrie-Fuller (Johnson *et al.* 1975) and Cisowski (1981) tests for the CMP rocks. Parameter *R* is the crossing point of IRM acquisition and demagnetization curves. Hcr is obtained projecting *R* on the abscissa.

indicating strong contribution of SP particles. However, values of Kfd $>$ 15 per cent are relatively rare in natural samples (Muxworthy 2001) and the obtained anomalously high values for granites deserve more investigation as they are not compatible with the MD magnetite grains indicated by the Lowrie–Fuller test. They may rather indicate misreading problems or to inclusions in iron-rich biotite, which are known to exhibit a wide range of grain sizes from SP to MD (Dunlop & Özdemir 1997).

Kfd could be a good indicator of CRM carried by the nucleation and growth of maghemite through the superparamagnetic threshold (Gendler *et al.* 2005). In our case contribution of SP grains is only significant in granites for which no major presence of titanomaghemite was noticed. For the other rocks for which maghemite was clearly identified the Kfd values did not indicate the possibility of any CRM in the SP threshold size.

5.4 SEM analyses

Nature and origin of the ferromagnetic minerals in the CMP rocks were investigated by SEM study (Figs 9 and 10). Most iron-bearing minerals of Cabo granites correspond to coarse titanohematite ($>$100 μm). Crystals show either high-temperature exsolution textures (ilmenite) or euhedral and well preserved tabular structure (Figs 9a–e). Because temperatures interpreted for the eutectoid reaction that marks the beginning of hematite-ilmenite exsolution vary between 390 and 520 °C depending of the authors, the exsolved

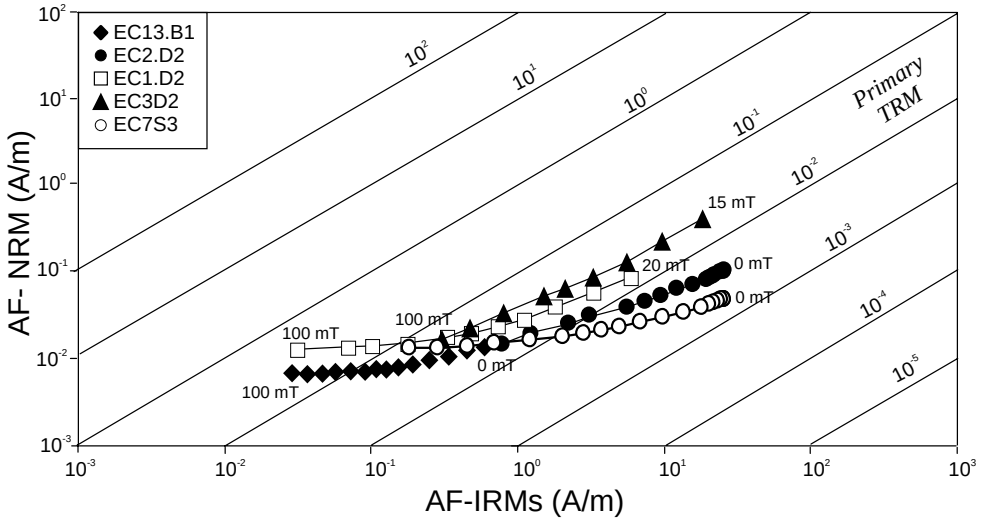

Figure 8. NRM:IRM ratios after AF demagnetization processes. CMP rocks exhibit NRM:IRM ratios close to 10^{-2}, typical of rocks carrying Thermal Remanent Magnetization (Fuller *et al.* 2002).

hematite should carry a CRM acquired during cooling-exsolution. Magnetite was not successfully observed probably because it correspond to a very fine-grained population near the superparamagnetic domain as suggested by Kfd values and Lowrie–Fuller test. Zircon is accessorily present both with Ti-free iron oxides and very altered pyrite (Figs 9f–h).

Magnetic minerals in rhyolites are essentially larger (>20 μm) and smaller (~ 5 μm) titanomagnetites (Figs 10a and b). The former exhibit exsolution textures of magnetite-ilmenite intergrowths typical of high-temperature oxidation and pointing to a primary nature for this mineral. Fine-grained iron oxides have the typical spinel octahedral structure. Identical well-preserved octahedra dominate the magnetic mineralogy of trachy-andesite and probably correspond to titanomagnetite accordingly to magnetic results (Figs 10c and d). Trachytes contain large (60–80 μm) Ti-iron oxides with typical exsolution structures. Hexagonal and tabular structures point to presence of titanohematite. In monzonites, large (100–200 μm) iron oxides, for which cubic structure indicate titanomagnetite, had suffered important alteration (weathering?), and do not exhibit exsolution textures.

5.5 Anisotropy of magnetic susceptibility

AMS fabrics were evaluated for granites (eight sites), monzonites (two sites), rhyolites (five sites) and ignimbrites (one site). Jelinek (1981) parameters (corrected degree of anisotropy *P'* and shape parameter *T*) were used to characterize the magnetic fabric. The orientation of the mean magnetic susceptibility ellipsoid with the associated uncertainties was determined by the tensor variability (Hext 1963; Jelinek 1978).

Granites display low values of *K* (25–250 $\times$ 10^{-6} SI) suggesting a significant contribution of paramagnetic carriers for the resultant AMS fabric (Tarling & Hrouda 1993; Borradaile & Henry 1997). The magnetic ellipsoid mainly exhibits low anisotropy values ($P' < 1.03$) with shape varying from moderate prolate to oblate (Fig. 11). For most samples K_3 is well clustered while K_1 and K_2 are scattered along a great circle defining the magnetic foliation. Such magnetic foliation roughly follows the morphology of the Cabo Massif (Fig. 11).

Monzonites show low bulk susceptibility values varying from 200 to 500 $\times$ 10^{-6} SI. Samples show well-defined K_3 while K_1 andK_2 are distributed along an E–W foliation plane plunging deeply towards S. This magnetic fabric is similar to the orientation of the rhyolitic dyke located close to theses samples (Fig. 1). *K* values of rhyolites are up to 4.0 $\times$ 10^{-3} SI with $P' < 1.10$. Ellipsoid shapes vary from oblate to prolate and axes indicate a magnetic foliation mostly plunging towards WNW. The exception is found for site EC-19, which shows a subhorizontal foliation slightly plunging towards NE, similar to the orientation of the local rhyolitic sill. The ignimbrite display relatively high *K* values (between 10^{-3} and 10^{-2} SI) with predominantly oblate ellipsoids defining a nearly horizontal magnetic foliation which is compatible with the depositional mechanism of the hot particles in suspension in the atmosphere (Tarling & Hrouda 1993). In conclusion, the CMP rocks have relatively low *K*-values but are likely to exhibit primary AMS pattern resulting from intrusion/eruption processes in the province.

6 DISCUSSION

6.1 Nature and origin of the magnetization: TRM, CRM or both?

Magnetic mineralogy data for most CMP rocks points to a primary origin for the characteristic remanence, which is consistent with the Cretaceous Normal Superchron. Main magnetic carriers are titanomagnetite and titanohematite. The latter occurs mainly in granites being responsible for about 30 per cent of the remanence after AF demagnetization. However, both minerals carry the same magnetization component indicating that hematite formed at high temperatures. A smaller harder fraction noticed in the IRM acquisition and demagnetization curves may be of secondary origin and carry a chemical remanence. In spite of all the evidences of a thermal origin for the characteristic magnetizations, the presence of a reversed component C in some rhyolite samples must be interpreted with caution. Component C is identified from temperatures of about 350 °C, coinciding with the inversion temperatures of maghemite into hematite (Figs 4e–j). Above 580 °C remanence tend to realign with component A or to become random as intensities reach the detection limit of the magnetometer. Apparently the new-formed hematite acquired a self-reversed magnetization. However, during AF demagnetization, when no maghemite inversion is expected, the magnetization vector tends to a reversed component for higher fields

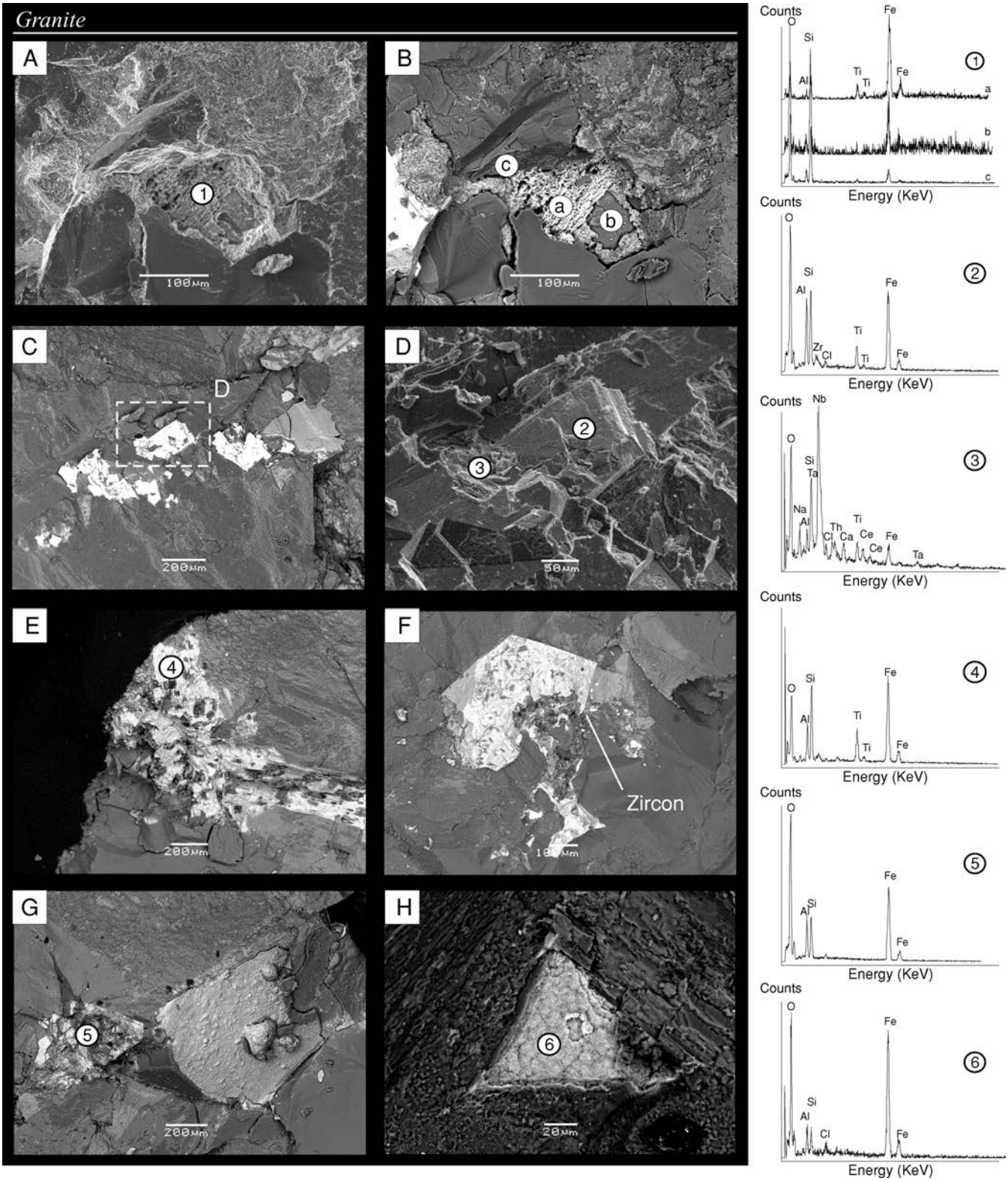

Figure 9. Scanning electron microscopy (SEM) photographs of Cabo Granites (EC8) showing predominance of titanohematite. Iron-bearing minerals are identified by back-scattered electron composition: bright zones correspond to heavy minerals for which composition is given by EDS spectra (on the right). Associated secondary electron image provides information about the morphology of the crystals. Titanohematites are characterized by severe exsolutions textures (a, b) but could also present well-preserved euhedral structures free of any exsolution (c, d). Some Ti-iron oxides show much altered states (e). Zircon (f), Ti-free iron oxides (g) and severely oxidized pyrite (h) are also encountered.

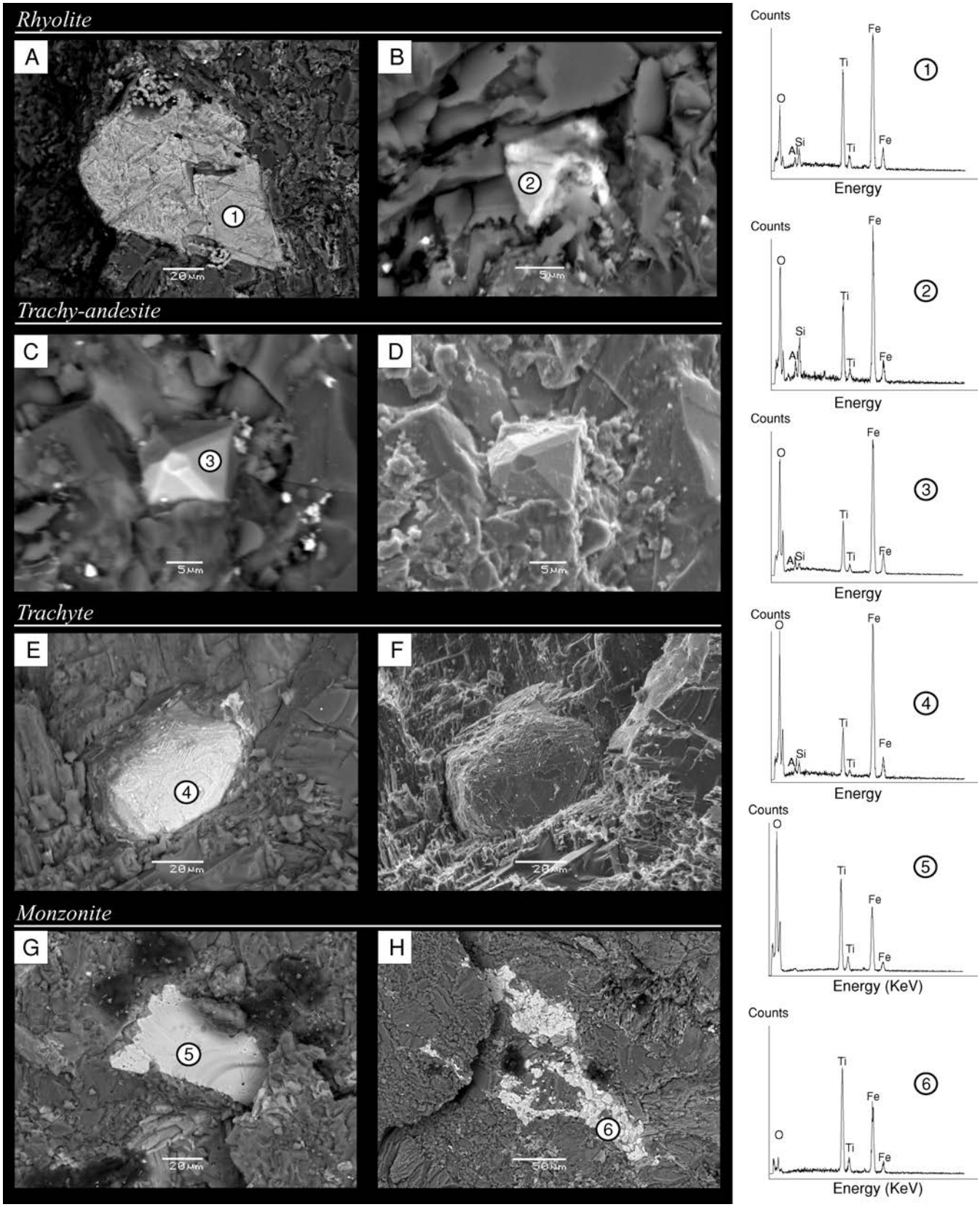

Figure 10. SEM photographs of CMP rocks. Rhyolites are characterized by mixture of large titanomagnetite with magnetite-ilmenite exsolutions (a) and smaller octahedral corroded titanomagnetite (b). Similar octahedral titanomagnetite is the unique magnetic carrier in Trachy-andesite (c, d): Trachytes contain large Ti-iron oxides with exsolutions assigned to be titanohematite (e, f). Magnetic minerals in monzonites correspond to altered titanomagnetite without any exsolution texture (g, h).

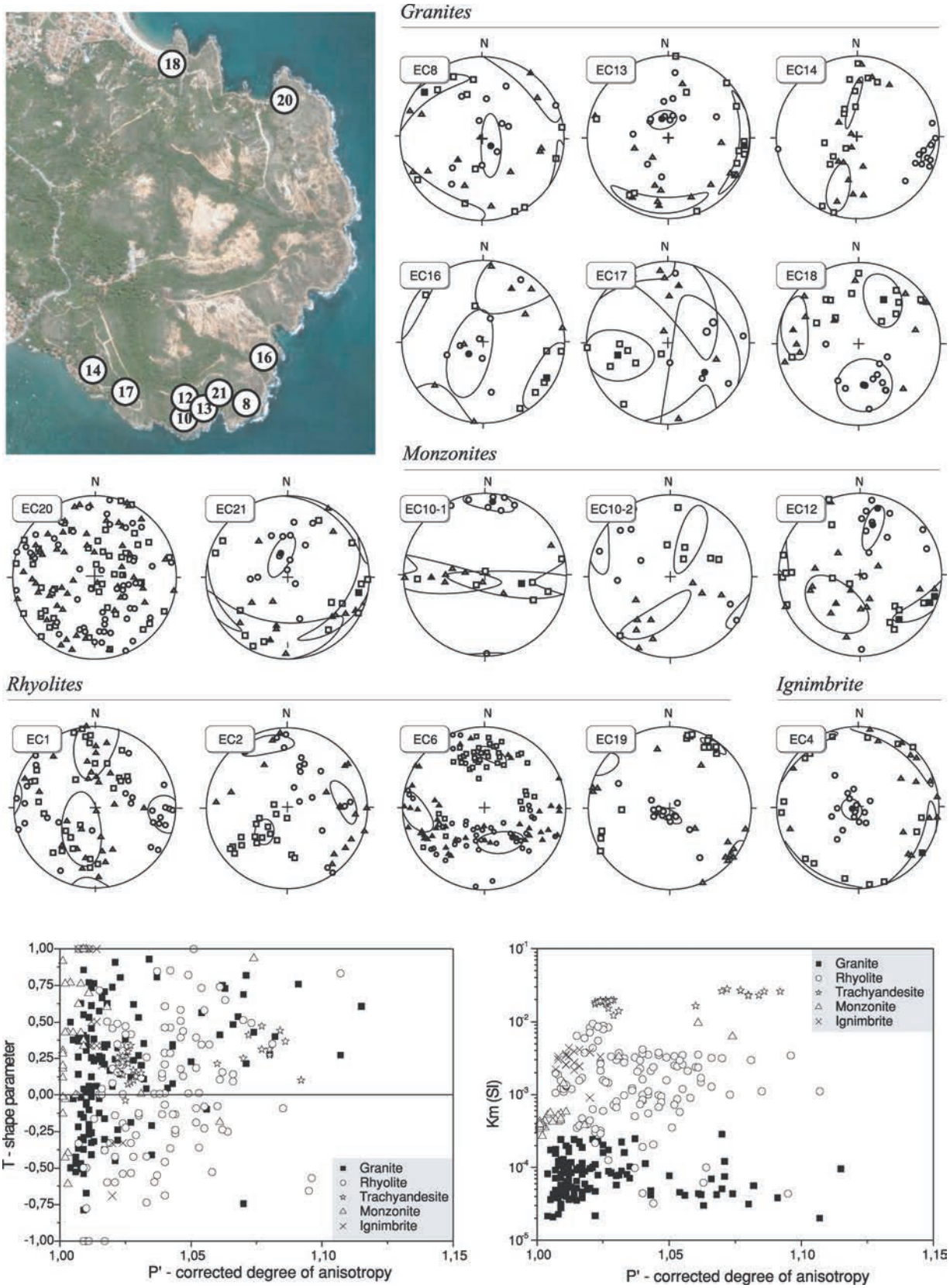

Figure 11. Anisotropy of Magnetic Susceptibility data of Cabo Granites and their geographical localization within the Cabo Santo Agostinho Massif. AMS data of rhyolites, monzonites and ignimbrites are also shown (see Fig. 1 for location). Stereographic projections for each palaeomagnetic site are shown with their respective magnetic susceptibility ellipsoid axes: maximum K_1 (squares), intermediate K_2 (triangles) and minimum K_3 (circles). Diagrams of shape parameter (T; Jelinek 1981) versus corrected degree of anisotropy (P') and mean susceptibility (km) versus P' are also shown (outliers values with $P > 1.15$ were removed).

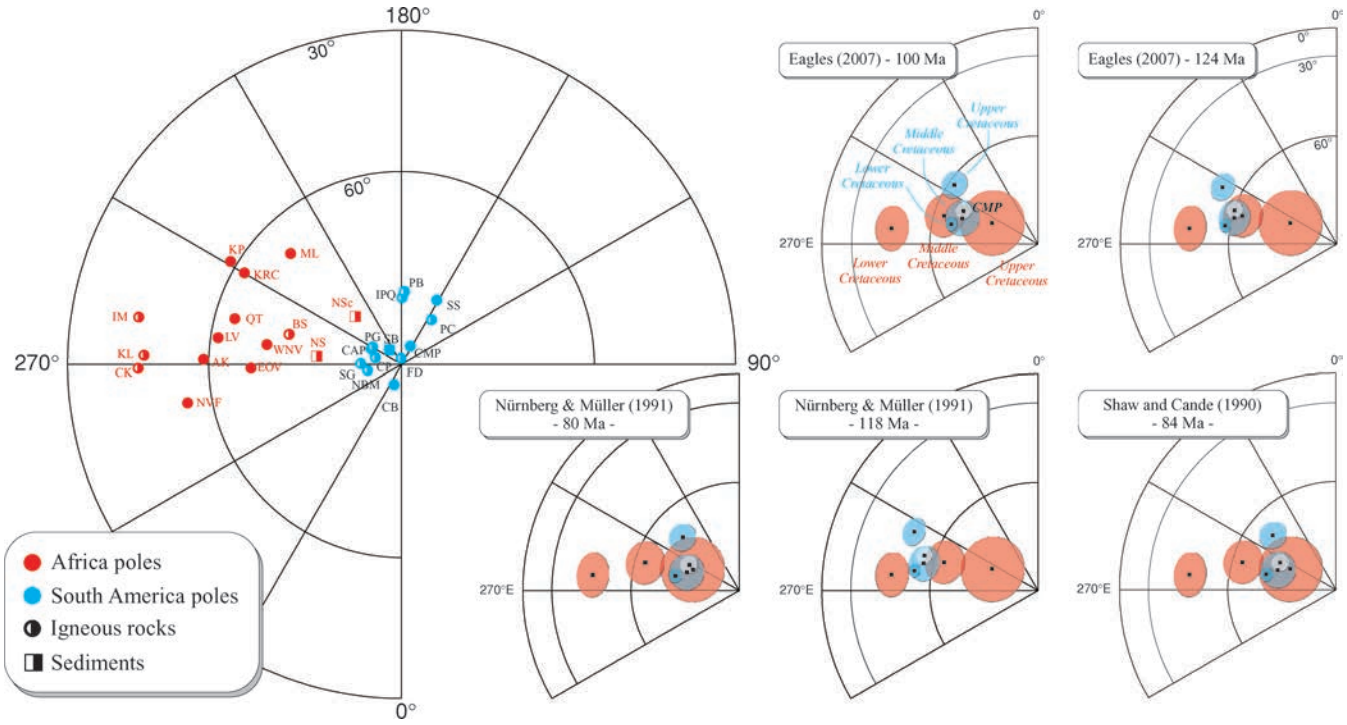

Figure 12. Virtual Geomagnetic Pole for Africa (red) and South America (blue) plotted on the North Hemisphere (left-hand corner) (*cf*. Table 4). Mean cretaceous palaeomagnetic poles for Africa and South America rotated to Africa using rotations pole from Eagles (2007), Nürnberg & Müller (1991) and Shaw & Cande (1990) are shown. Filled and semi-filled symbols represent normal and mixed polarities, respectively. Palaeomagnetic pole of the CMP is also shown.

(EC5A; Fig. 2). It is possible that a secondary magnetization was acquired during a short reversed event within the Cretaceous Normal Superchron or later. A possible explanation for the origin of the reversed component bears on self-reversal processes as described for highly oxidized MORB basalts (Doubrovine & Tarduno 2004, 2005; Krása & Matzka 2007) but it deserves further investigation.

6.2 Testing Cretaceous kinematic models for South Atlantic

The palaeomagnetic pole for CMP obtained in this study supersedes the Cabo de Santo Agostinho pole previously presented by Schult & Guerreiro (1980). The new pole includes all sites investigated by those authors besides various sites of granite and monzonite rocks not studied before. This pole satisfies most of the quality criteria of Van der Voo (1990) in the sense it has (1) good radiometric age control, (2) statistically well determined magnetic direction obtained through analysis of an adequate number of samples over a significant geographic area, (3) detailed demagnetization demonstrating the isolation of the characteristic magnetization through vector subtraction and (4) structural continuity of the studied region with the craton it represents. The criteria (5), originally corresponding to the distinctiveness of the reported palaeomagnetic direction from more recent magnetic overprints, is replaced by a complete rock magnetic study because of the proximity of Cretaceous poles to the present pole. Only field test and presence of reversal are needed to completely fulfil all requirements for a maximum quality classification $Q = 7$. However, it has been demonstrated that large geomagnetic variations (possibly associated to reversals within Cretaceous Normal Superchron already reported in literature) were recorded by various lithologies in distinct sampling sites, and comparison of magnetic directions among different sites plus valuable information from AMS guarantee that rocks have not been deformed and are able to preserve primary magnetization.

The CMP pole plots (Fig. 12a) close to the San Bernardo pole given by Somoza & Zaffarana (2008) also of mid-Cretaceous age and normal polarity. Early- to mid-Cretaceous poles for South America cluster near the geographic pole indicating that no significant rotation occurred during the elapsed time. However, considering the number and quality of the available poles a net distinction between Early- and mid-Cretaceous is possible, and therefore, for the purpose of this paper we will consider three mean poles corresponding to Early, mid and Late Cretaceous (Table 4).

The International Association of Geomagnetism and Aeronomy database records many palaeomagnetic poles for Africa for the same time interval (Table 4), although not all of them rank highly in quality assessments. These poles seem scattered when plotted in Fig. 12 even considering only data from igneous rocks in order to minimize uncertainties in the palaeomagnetic record of sedimentary rocks due to problems of shallowing and time of magnetization acquisition. Excepting the three Early Cretaceous poles that form a group easily distinguishable from the others, most of the selected poles have poorly constrained dating within intervals of 40 Myr or greater making difficult the discrimination of age groups. Therefore, we used the criterion of magnetic polarity for calculating mean poles for Early (mixed polarities), mid (normal polarity) and Late (normal and mixed) Cretaceous, based on the polarity pattern of South America poles. Note that in Fig. 12 South America and Africa poles are displayed as north poles in the present-day configuration.

The mean poles for both continents were compared by rotating South American poles to Africa according to various models of

Table 4. Cretaceous palaeomagnetic poles for South America.

Formation	Code	Age (Ma)	Pol.	*N*	Long. (°E)	Lat. (°N)	References
Africa							
Nubian Sandstone Combined	NSc	65–100	N/R	22	220.0	79.0	Schult *et al.* (1978)
Basalt Series I	BS	65–100	N/R	12	251.0	72.0	Storetvedt *et al.* (1978)
Nubian Sandstone	NS	65–101	N/R	82	259.0	77.0	Hussain & Aziz (1983)
Quseir Trachytes	QT	63–92	N	16	252.0	63.0	Ressetar *et al.* (1981)
East El Oweinat Volcanics	EOV	65–102	N	10	268.0	67.0	Hussain & Aziz (1983)
El Khafa Ring Complex	KRC	74–95	N	4	238.0	61.0	Ressetar *et al.* (1981)
Northern Volcanic Field	NVF	78–83	N	6	277.8	56.0	Saradeth *et al.* (1989)
Kimberlite pipes	KP	81–87	N	5	237.0	58.0	McFadden & Jones (1977)
Monastery-Lesotho kimberlites	ML	84–92	N	6	223.0	65.0	Hargraves & Onstott (1980)
Wadi Natash Volcanics	WNV	86–100	N	15	258.0	69.0	Schult *et al.* (1981)
Abu Khrug Ring Complex	AK	87–91	N	6	266.0	59.0	Ressetar *et al.* (1981)
Lupata Series Volcanics	LV	109–113	N	7	259.0	61.0	Gough & Opdyke (1963)
Intrusives, Morocco	IM	110–130	N/R	4	258.0	46.0	Westphal *et al.* (1979)
Kaoko lavas	KL	112–131	N/R	40	266.0	48.0	Gidskehaug *et al.* (1975)
Cretaceous Kimberlites comb.	CK	113–145	N/R	10	269.0	47.0	Hargraves (1989)
Mean Africa Poles							
Upper Cretaceous		65–80	N/R	3	245.5	76.5	$A_{95} = 8.8$; $K = 196$
Middle Cretaceous		80–110	N	9	253.5	63.1	$A_{95} = 5.9$; $K = 76$
Lower Cretaceous		110–140	N/R	3	264	47	$A_{95} = 6.1$; $K = 406$
South America (North Pole)							
Patagonian Basalts	PB	64–79	N/R	18	178.4	78.7	Butler *et al.* (1991)
Itatiaia and Passa Quatro comb.	IPQ	70–71	N/R	18	180.0	79.5	Montes-Lauar *et al.*(1995)
Poços de Caldas Complex	PC	84	N/R	36	145.7	82.2	Montes-Lauar *et al.*(1995) recalc.
São Sebastião Dykes	SS	80–90	N	26	151.3	79.0	Montes-Lauar *et al.*(1995)
San Bernardo	SB	85–98	N	9	215.0	87.0	Somoza & Zaffarana (2008)
Cabo Magmatic Province, Brazil	CMP	100	N	24	155.9	87.9	This paper
Cerro Barcino, Argentina	CB	112–130	N	16	339.0	87.0	Geuna *et al.* (2000)
Florianópolis Dykes, SE Brazil	FD	119–128	N/R	65	183.3	89.1	Raposo *et al.* (1998)
Central Alkaline Province	CAP	127–130	N/R	75	242.3	85.4	Ernesto *et al.* (1996)
Ponta Grossa Dikes, SE Brazil	PG	129–131	N/R	115	238.5	84.5	Ernesto *et al.* (1999)
Serra Geral Formation	SG	133–132	N/R	392	269.2	84.1	Ernesto *et al.* (1990, 1999)
Cordoba Province, Argentina	CP	133–115	N/R	55	255.9	86.0	Geuna & Vizán (1998)
Northeastern Brazil Magmatism	NBM	125–145	N/R	44	277.6	85.2	Ernesto *et al.* (2002)
Mean South America Poles							
Upper Cretaceous		65–80	N/R	4	165.2	80.2	$A_{95} = 3.9$; $K = 552$
Middle Cretaceous		80–110	N	3	230.9	89.2	$A_{95} = 4.9$; $K = 646$
Lower Cretaceous		110–140	N/R	6	254.8	86	$A_{95} = 1.9$; $K = 1152$

South Atlantic opening (Fig. 12). Early Cretaceous poles represent the pre-drift configuration and will be not discussed here. The mid-Cretaceous mean poles for South America were rotated using the Euler poles given by Eagles (2007), Shaw & Cande (1990) and Nürnberg & Müller (1991) as they differ significantly. Several Euler poles plot very near (Bullard family according to Eagles 2007), and are based on similar methodologies, therefore we used the Nürnberg and Müller's poles as representative of the family. Considering age uncertainties both on mean palaeomagnetic poles and Euler poles, we tested reconstructions from 124 to 84 Ma, and results are seen in Fig. 12. It becomes clear that the best adjustment for mid-Cretaceous is achieved with the 124 Ma model of Eagles. His 100 Ma (anomaly C34i corresponding to halfway anomaly C34) places the mid-Cretaceous pole for South America in between the African mid- and Late Cretaceous poles. Even if we consider the well-calibrated CMP (age 102 Ma) pole alone the situation does not change. This is probably due to the uncertainties in the age interval of the selected poles included in the means. The Nürnberg & Müller's (1991) pole of 118 Ma does not solve the problem, on the contrary, the mid-Cretaceous pole for South America is completely inserted within the confidence circle of the Late Cretaceous pole of Africa. These results indicate that the model presented by Eagles is a better representation of that stage of the South Atlantic formation.

Shaw & Cande (1990) considered the end of the anomaly at 84 Ma (C34y), for that age the mean palaeomagnetic poles do not match although the circle of confidence of the African poles is large. The best adjustment is given by the Nürnberg & Müller's (1991) 80 Ma pole and only a partial superposition is produced by this rotation. Once again we must have in mind the large uncertainties that still exist in the Late Cretaceous positions of the two continents; there are still few palaeomagnetic poles and in most cases ages are not well constrained. Therefore, the mean poles are probably mixing ages within a 30–40 Ma interval, as clearly seen in Table 4.

Better fits between South America and Africa in pre-drift configuration were achieved considering intraplate deformations (Unternehr *et al.* 1988; Schettino & Scotese 2005) as a consequence of the ∼34 Ma diachronous opening of South Atlantic from south to north. Accommodation zones are believed to be active from Late Jurassic to Lower Cretaceous (Hauterivian) causing relative

movements of about 200 km (∼2°). This is within the statistical errors of most of the palaeomagnetic poles or mean poles and, depending on the fault strike relative to the geographic axis, no variation in palaeolatitude will be produced, and the poles will be insensitive to these movements. Anyway, the most affected palaeomagnetic poles would be those of Early Cretaceous ages. Therefore, the misfit of mean poles cannot be attributed to the effects of uncorrected deformations, mainly if the CMP pole is taken alone as it is well constrained in age. Furthermore, the errors would be smaller than the uncertainties in pole determinations.

7 CONCLUSIONS

All volcanic and plutonic rocks of the CMP showed stable demagnetization patterns in high temperatures and high AF-demagnetizing field. NRM to IRM ratios and presence of typical magnetite-ilmenite exsolutions textures suggest that most of the primary magnetic mineralogy have been preserved in the CMP rocks. Both primary titanomagnetite and titanohematite are the magnetic carriers of TRM and high temperature CRM, respectively, in granites and trachytes, whereas in monzonites and rhyolites, the remanence is carried by mixtures of titanomagnetite and titanomaghemite. Characteristic magnetization directions are mostly of normal polarity (component A) but some sites displayed another component (B) compatible with an anomalous or transitional field. A third component (C) of positive inclinations was identified in samples from sites EC5 and EC6 but it is probably of chemical origin due to weathering and was discarded for the calculation of the palaeomagnetic pole. This new pole (CMP) supersedes the Cabo de Santo Agostinho palaeomagnetic pole given by Schult & Guerreiro (1980) and can be considered as a high quality palaeomagnetic pole ($Q = >5$) for the mid-Cretaceous and is a reference pole for South America at ∼100 Ma.

The tests of the kinematic models for the South Atlantic opening favoured the Eagles (2007) pole at 124 Ma as a better representation of the mid-Cretaceous stage. This age was believed to mark the beginning of the CNS, and in order to calculate the 100 Ma rotation pole the author considered the middle of anomaly 34, assuming constant velocities of crust formation on both sides of the meso-Atlantic ridge. This assumption may constitute a source of error, justifying, at least in part, the misfit between the South America and Africa mean poles using his 100 Ma rotation pole. However, the database for both continents still needs improvement, especially on the African side: the poor definition of ages is the main difficult in defining the mean palaeomagnetic poles. To overcome the trouble we used the magnetostratigraphy, which resulted in a good criterion. As easily noticed in Fig. 12 the dispersion of mid Cretaceous African poles (normal polarity) is essentially in longitude and is probably related to problems in eliminating secular variation, as six out of nine poles are based on less than 10 sites. The misfit of the mean poles using the different Atlantic opening models is mainly in latitude.

ACKNOWLEDGMENTS

This work was supported by FAPESP (grants 05/059674–4 and 05/52518–7). We thank Cor Langereis, Greame Eagles and Silvana Geuna for their constructive reviews, which improved the original version of the manuscript. Thanks are due to technicians and researchers of the LMTG (Toulouse, France): Thierry Aigouy, Philippe de Perceval, Sophie Gouy for SEM analyses; Jean-Luc Bouchez and Anne Nédélec for numerous discussions. We thank Miguel Carminatti and Edson José for helping during field work and Everton Frigo.

REFERENCES

Borradaile, G.J. & Henry, B, 1997. Tectonic applications of magnetic susceptibility and its anisotropy, *Earth Sci. Rev.*, **42**(1–2), 49–93.

Butler, R.F., Hervé, F., Munizaga, F., Beck, M.E. Jr., Burmester, R.F. & Oviedo, E.S., 1991. Paleomagnetism of the Patagonian plateau basalts, southern Chile and Argentina, *J. geophys. Res.*, **96,** 6023–6034.

Cisowski, S., 1981. Interacting vs. non-interacting single domain behaviour in natural and synthetic samples, *Phys. Earth planet. Inter.*, **26,** 56–62.

Doubrovine, P.V. & Tarduno, J.A., 2004. Self-reversed magnetization carried by titanomaghemite in oceanic basalts, *Earth planet. Sci. Lett.*, **222**(3–4), 959–969.

Doubrovine, P.V. & Tarduno, J.A., 2005. On the compositional field of self-reversing titanomaghemite: constraints from Deep Sea Drilling Project site 307, *J. geophys. Res.*, **110,** B11104, doi:10.1029/2005JB003865.

Dunlop, D. & Özdemir, Ö., 1997. *Rock Magnetism: Fundamentals and Frontiers, Cambridge Studies in Magnetism*, Cambridge University Press, Cambridge.

Eagles, G., 2007. New angles on South Atlantic opening, *Geophys. J. Int.*, **168**(1), 353–361.

Ernesto, M., Pacca, I.G., Hiodo, F.Y. & Nardy, A.J.R, 1990. Paleomagnetism of the Mesozoic Serra Geral Formation, Southern Brazil, *Phys. Earth planet. Inter.*, **64**(2–4), 153–175.

Ernesto, M., Comin-Chiaramonti, P., Gomes, C.B., Piccirillo, E.M., Castillo, A.M.C. & Velázquez, J.C., 1996. Paleomagnetic data from the Central Alkaline Province, Eastern Paraguay, in *Alkaline Magmatism in Central-Eastern Paraguay. Relationships with coeval magmatism in Brazil*, pp. 85–102, eds Comin-Chiaramonti, P. & Gomes, C.B., Edusp/Fapesp, São Paulo, Brazil.

Ernesto, M., Raposo, M.I.B., Marques, L.S., Renne, P.R., Diogo, L.A. & De Min, A., 1999. Paleomagnetism, geochemistry and 40Ar/39Ar dating of the North-eastern Paraná Magmatic province: tectonic implications, *J. Geodyn.*, **28,** 321–340.

Ernesto, M., Bellieni, G., Piccirillo, E.M, Marques, L.S., De Min, A., Pacca, I.G., Martins, G. & Macedo, J.W.P., 2002. Paleomagnetic, geochronological and geochemical constraints on time and duration of the Mesozoic igneous activity in Northeastern Brazil, in *The Central Atlantic Magmatic Province*, AGU Monograph 136, pp. 129–149, Am. Geophys. Un., doi:10.1029/136GM07.

Fisher, R., 1953. Dispersion on a sphere, *Proc. R. Soc. Lond., Ser. A,* **217,** 295–305.

Fuller, M., Cisowski, S., Hart, M., Haston, R., Schmidtke, E. & Arrard, R., 1988. NRM:IRM(S) demagnetization plots: an aid to the interpretation of natural remanent magnetization, *Geophys. Res. Lett.*, **15,** 518–521.

Fuller, M., Kidane, T. & Ali, J., 2002. AF demagnetization characteristics of NRM, compared with anhysteretic and saturation isothermal remanence: an aid in the interpretation of NRM, *Phys. Chem. Earth,* **27,** 1169–1177.

Gendler, T.S., Shcherbakov, V.P., Dekkers, M.J., Gapeev, A.K., Gribov, S.K. & McClelland, E., 2005. The lepidocrocite–maghemite–hematite reaction chain–I. Acquisition of chemical remanent magnetization by maghemite, its magnetic properties and thermal stability, *Geophys. J. Int.*, **160,** 815–832.

Geuna, S.E. & Vizán, H., 1998. New Early Cretaceous palaeomagnetic pole from Córdoba Province (Argentina): revision of previous studies and implications for the South American database, *Geophys. J. Int.*, **135,** 1085–1100.

Geuna, S.E., Somoza, R., Vizan, H., Figari, E.G. & Rinaldi, C.A., 2000. Paleomagnetism of Jurassic and Cretaceous rocks in central Patagonia: a key to constrain the timing of rotations during the breakup of southwestern Gondwana? *Earth planet. Sci. Lett.*, **181**(1–2), 145–160.

Gidskehaug, A., Creer, K.M. & Mitchell, J.G., 1975. Paleomagnetism and K-Ar Ages of Southwest African Basalts and their bearing on time of initial rifting of South-Atlantic Ocean, *Geophys. J. R. astr. Soc.*, **42**(1), 1–20.

Gough, D.I. & Opdyke, N.D., 1963. The palaeomagnetism of the Lupata alkaline volcanics, *Geophys. J. R. astr. Soc.*, **7**(4), 457–468.

Gradstein, F.M., Ogg, J.G., Smith, A.G., Bleeker, W. & Lourens, L.J., 2004. A new geologic time scale, with special reference to Precambrian and Neogene, *Episodes*, **27**(2), 83–100.

Gvirtzman, G., Weissbrod, T., Baer, G. & Brenner, G.J., 1996. The age of the Aptian Stage and its magnetic events: new Ar-Ar ages and paleomagnetic data from the Negev, Israel, *Cretaceous Res.*, **17,** 293–310.

Hargraves, R.B., 1989. Paleomagnetism of Mesozoic kimberlites in Southern-Africa and the Cretaceous Apparent Polar Wander curve for Africa, *J. geophys. Res.*, **94**(B2), 1851–1866.

Hargraves, R.B. & Onstott, T.C., 1980. Paleomagnetic results from some Southern African Kimberlites, and their tectonic significance, *J. geophys. Res.*, **85**(B7), 3587–3596.

He, H., Pan, Y., Tauxe, L., Qin, H. & Zhu, R., 2008. Toward age determination of the M0r (Barremian–Aptian boundary) of the Early Cretaceous, *Phys. Earth planet. Inter.*, **169,** 41–48.

Hext, G., 1963. The estimation of second-order tensor, with related tests and designs, *Biometrika*, **50,** 353–357.

Hussain, A.G. & Aziz, Y., 1983. Paleomagnetism of mesozoic and tertiary rocks from east El-Owenat area, Southwest Egypt, *J. geophys. Res.*, **88**(B4), 3523–3529.

Irving, E. & Archibald, D.A., 1990. Bathozonal tilt corrections to paleomagnetic data from Mid-cretaceous Plutonic Rocks—examples from the Omineca Belt, British-Columbia, *J. geophys. Res.*, **95**(B4), 4579–4585.

Jelinek, V., 1978. Statistical processing of aniosotropy of magnetic-susceptibility measured on groups of specimens, *Stud. Geophys. Geod.*, **22,** 50–62.

Jelinek, V., 1981. Characterization of the magnetic fabric of rocks, *Tectonophysics*, **79,** 63–67.

Johnson, H.P., Lowrie, W. & Kent, D.V., 1975. Stability of anhysteretic remanent magnetization in fine and coarse magnetite and maghemite, *Geophys. J. R. astr. Soc.*, **41,** 1–10.

Kirschvink, J.L., 1980. The least-squares line and plane and the analysis of paleomagnetic data, *Geophys. J. R. astr. Soc.*, **62,** 699–718.

Krása, D. & Matzka, J., 2007. Inversion of titanomaghemite in oceanic basalt during heating, *Phys. Earth planet. Inter.*, **160,** 169–179.

Kruiver, P.P., Dekkers, M.J. & Heslop, D., 2001. Quantification of magnetic coercivity components by the analysis of acquisition curves of isothermal remanent magnetization, *Earth planet. Sci. Lett.*, **189,** 269–276.

Lima Filho, M.F., 1998. Análise estratigráfica e estrutural da Bacia Pernambuco, *Tese de Doutorado,* Instituto de Geociências, Universidade de São Paulo, São Paulo, 139 pp.

Lima Filho, M.F. & Szatmari, P., 2002. Ar-Ar geochronology of volcanic rocks of the Cabo Magmatic Province (CMP)—Pernambuco Basin. II Simpósio sobre Vulcanismo e Ambientes Associados, Belém/PA, Resumos, pp. 59–59.

Long, L.E., Sial, A.N., Ekvanil, H.E. & Borba, G.S., 1986. Origin of granite at Cabo de Santo Agostinho, Northeast Brazil, *Contrib. Mineral. Petrol.*, **92,** 341–350.

Mcfadden, P.L. & Jones, D.L., 1977. Paleomagnetism of some Upper Cretaceous Kimberlite occurrences in South-Africa, *Earth planet. Sci. Lett.*, **34**(1), 125–135.

Montes-Lauar, C.R., Pacca, I.G., Melfi, A.J. & Kawashita, K., 1995. Late Cretaceous alkaline complexes, southeastern Brazil: Paleomagnetism and geochronology, *Earth planet. Sci. Lett.*, **134,** 425–440.

Muxworthy, A.R., 2001. Effect of grain interactions of the frequency dependence of magnetic susceptibility, *Geophys. J. Int.*, **144,** 441–447.

Nascimento, M.A.L., 2003. Geologia, geocronologia, geoquímica e petrôgenese das rochas ígneas cretacícas da Provincia Magmática do Cabo e sua relações com as unidades sedimentares da Bacia de Pernambuco (NE Brasil), *Tese (Doutorado em Geociências)*, Universidade Federal do Rio Grande do Norte, Natal, pp. 233.

Nürnberg, G.D. & Müller, R.D., 1991. The tectonic evolution of the South-Atlantic from Late Jurassic to present, *Tectonophysics*, **191**(1–2), 27–53.

Poornachandra Rao, G.V.S. & Mallikharjuna Rao, J., 1996. Palaeomagnetism of the Rajmahal Traps of India: implication to the reversal in the Cretaceous Normal Superchron, *J. Geomag. Geoelectr.*, **48**(7), 993–1000.

Raposo, M.I.B., Ernesto, M. & Renne, P.R., 1998. Paleomagnetic and $^{40}Ar/^{39}Ar$ data on the Early Cretaceous dyke swarm from the Santa Catarina island, Southern Brazil, *Earth planet. Sci. Lett.*, **144,** 199–211.

Ressetar, R., Nairn, A.-E.M. & Monrad, J.R., 1981. 2 Phases of Cretaceous-Tertiary Magmatism in the Eastern Desert of Egypt–paleomagnetic, chemical and K-Ar evidence, *Tectonophysics*, **73**(1–3), 169–193.

Robertson, D.J. & France, D.E., 1994. Discrimination of remanence-carrying minerals in mixtures, using isothermal remanent magnetisation acquisition curves, *Phys. Earth planet. Inter.*, **82,** 223–234.

Saradeth, S., Soffel, H.C., Horn, P., Mullersohnius, D. & Schult, A., 1989. Upper Proterozoic and Phanerozoic pole positions and Potassium Argon (K-Ar) ages from the East Sahara Craton, *Geophys. J.*, **97**(2), 209–221.

Schettino, A. & Scotese, C.R., 2005. Apparent polar wander paths for the major continents (200 Ma to the present day): a palaeomagnetic reference frame for global plate tectonic reconstructions, *Geophys. J. Int.*, **163,** 727–759.

Schult, A. & Guerreiro, S.D.C., 1980. Paleomagnetism of upper cretaceous volcanic-rocks from Cabo-de-Santo-Agostinho, Brazil, *Earth planet. Sci. Lett.*, **50**(1), 311–315.

Schult, A., Soffel, H.C. & Hussain, A.G., 1978. Paleomagnetism of cretaceous Nubian sandstone, Egypt, *J. Geophys.*, **44**(4), 333–340.

Schult, A., Hussain, A.G. & Soffel, H.C., 1981. Paleomagnetism of upper cretaceous volcanics and Nubian sandstones of Wadi-Natash, SE Egypt and implications for the polar wander path for Africa in the Mesozoic, *J. Geophys.*, **50**(1), 16–22.

Shaw, P.R. & Cande, S.C., 1990. High-resolution inversion for South-Atlantic plate kinematics using joint altimeter and magnetic anomaly data, *J. geophys. Res.*, **95**(B3), 2625–2644.

Somoza, R. & Zaffarana, C.B., 2008. Mid-cretaceous polar standstill of South America, motion of the Atlantic hotspots and the birth of the Andean Cordillera, *Earth planet. Sci. Lett.*, **271**(1–4), 267–277.

Storetvedt, K.M., Carmichael, C.M., Hayatsu, A. & Palmer, H.C., 1978. Paleomagnetism and K-Ar results from Duncansby volcanic neck, NE Scotland—superimposed magnetizations, age of igneous activity, and tectonic implications, *Phys. Earth planet. Sci.*, **16**(4), 379–392.

Tarduno, J.A., 1990. Brief reversed polarity interval during the Cretaceous Normal Polarity Superchron, *Geology*, **18**(8), 683–686.

Tarduno, J.A., Lowrie, W., Sliter, W.V., Bralower, T.J. & Heller, F., 1992. Reversed polarity characteristic magnetizations in the Albian Contessa section, Umbrian Apennines, Italy—implications for the existence of a Mid-Cretaceous mixed polarity interval, *J. geophys. Res.*, **97**(B1), 241–271.

Tarling, D.H. & Hrouda, F., 1993. *The Magnetic Anisotropy of Rocks*, Chapman & Hall, London.

Unternehr, P., Curie, D., Olivet, J.L., Goslin, J. & Beuzart, P., 1988. South Atlantic fits and intraplate boundaries in africa and south-america, *Tectonophysics*, **155**(1–4), 169–179.

Vandamme, D., 1994. A new method to determine paleosecular variation, *Phys. Earth planet. Inter.*, **85,** 131–142.

Van Der Voo, R., 1990. The reliability of paleomagnetic data, *Tectonophysics*, **184**(1), 1–9.

Vandenberg, J., Klootwijk, C.T. & Wonders, A.A.H., 1978. The late Mesozoic and Cenozoic movements of the Umbrian Peninsula: further palaeomagnetic data from the Umbrian Sequence, *Geol. Soc. Am. Bull.*, **89,** 133–150.

Vandoros, P., Cordani, U. & Matzko, J.J., 1966. Idades absolutas das rochas ígneas da região do cabo, in *SBG/Núcleo Sudeste*, Cong. Bras. Geol., Vol. 20, pp. 64–66, Vitória, Anais, 1.

Westphal, M., Montigny, R., Thuizat, R., Bardon, C., Bossert, A., Hamzeh, R. & Rolley, J.P., 1979. Paleomagnetism and K-Ar dating of Permian, Triassic, and Cretaceous rocks from Morocco, *Can. J. Earth Sci.*, **16**(11), 2150–2164.